Spatial distribution of centroid moment tensor solutions for the 2004 off Kii peninsula earthquakes

Yoshihiro Ito, Takumi Matsumoto, Hisanori Kimura, Hirotoshi Matsubayashi, Kazushige Obara, and Shoji Sekiguchi

National Research Institute for Earth Science and Disaster Prevention, 3-1, Tennodai, Tsukuba, Ibaraki 305–0006, Japan

(Received November 30, 2004; Revised March 9, 2005; Accepted March 22, 2005)

Two large intraplate earthquakes (M_W 7.0 and 7.3) occurred off the southeastern Kii Peninsula on September 5, 2004. We determined the centroid moment tensors of these earthquakes and their aftershocks. Earthquakes can be divided into two categories: (1) the reverse-fault type with a range in focal depth from 5 km to 20 km; and (2) earthquakes with a near-vertical nodal plane and a focal depth shallower than 5 km. Earthquakes of type (1) are distributed inside the Philippine Sea plate beneath the Nankai trough, while normal-fault events predominate in the other regions along the trough. The distribution of type (2) events shows two clear lineaments with strikes of NNW-SSE to the north and NE-SW to the west of the focal area. These lineament strikes coincide approximately with strikes at the nodal planes of such events.

Key words: Centroid moment tensor, broadband seismometer, tiltmeter, seismicity.

1. Introduction

Two large earthquakes with moment magnitudes (M_{JMA}) of 7.1 and 7.4 occurred off the Kii Peninsula in southeastern-central Japan at 10:07 and 14:57 (UT) on September 5, 2004. Their hypocenters were located near the eastern Nankai trough with focal depths of 37.58 km and 43.52 km, respectively (JMA: Japan Meteorological Agency, 2004). These focal depths are deeper than the plate boundary between the Philippine Sea plate and the Eurasian plate. Some results obtained by GPS, tsunami, or far-field wave analyses showed that the largest event had the complex source process (Hashimoto *et al*., 2005; Satake *et al*., 2005; Hara, 2005). The Philippine Sea plate subducts toward the northwest from the Nankai trough at a rate of approximately 4 cm/yr in this region (Seno *et al*., 1993) and large interplate thrust events with a recurrence interval of approximately 100 years also occur (Utsu, 1984). The most recent large event, the Tonankai Earthquake, had a magnitude of M_w 7.9 and occurred in 1944 (Kikuchi *et al*., 2003).

Lay *et al*. (1989) demonstrated the relationship between interplate thrusting and the stress field of the intraplate at the outer rise. They suggested that stresses in the outer rise might become compressional when interplate thrusting is locked. This study investigated the distribution of moment tensors of two large earthquakes and their intermediate-size aftershocks. We emphasize the type of focal mechanisms around the Nankai trough using the high dense broadband network established by the National Research Institute for Earth Science and Disaster Prevention (NIED).

2. Centroid Moment Tensor Inversion

The NIED F-net and Hi-net stations in Japan are spaced 100 km and 15–20 km apart, respectively (Okada *et al*., 2004). Three component broadband seismometers (STS-1/2) were installed at each F-net station and two horizontal-component borehole tiltmeters were installed at each Hi-net station. We used waveform data from the high dense broadband seismic stations to calculate centroid moment tensors (Fig. 1). The orientation of the observed borehole tiltmeter data was corrected by estimating the azimuth of the horizontal sensor as reported by Shiomi *et al*. (2003). Velocity seismograms and accelerograms with high S/N ratios obtained from the F-net and the Hi-net networks were converted to displacement and decimated to a 1 Hz sampling rate. Filters with pass-bands of 0.01–0.05 Hz and 0.02–0.05 Hz were used for the two large earthquakes and their aftershocks, respectively. To calculate Green's functions, we used the same velocity and Q structures employed for the routine NIED F-net moment tensor inversion approach (Fukuyama *et al*., 1998) (See Table 1).

Our approach for calculating the centroid moment tensors differs from the routine NIED F-net moment tensor inversion approach in the following respects: (1) The centroid hypocenter and time were calculated, whereas the fixed epicenter was obtained from the Japanese Meteorological Agency (JMA) Catalog. Centroid depth is estimated using this routine. (2) Waveform data from more than three F-net stations and two components of the tiltmeters at Hi-net stations were used in this study. Three F-net stations were used in the routine.

Under the point-source assumption, the centroid hypocenter and centroid time with maximum variance reduction (VR) were located around the initial hypocenter and origin time on a horizontal grid with spacing at 0.01 degrees. The vertical grids were spaced from 1 km down to 50 km on a time grid of 1 sec. The initial hypocenters

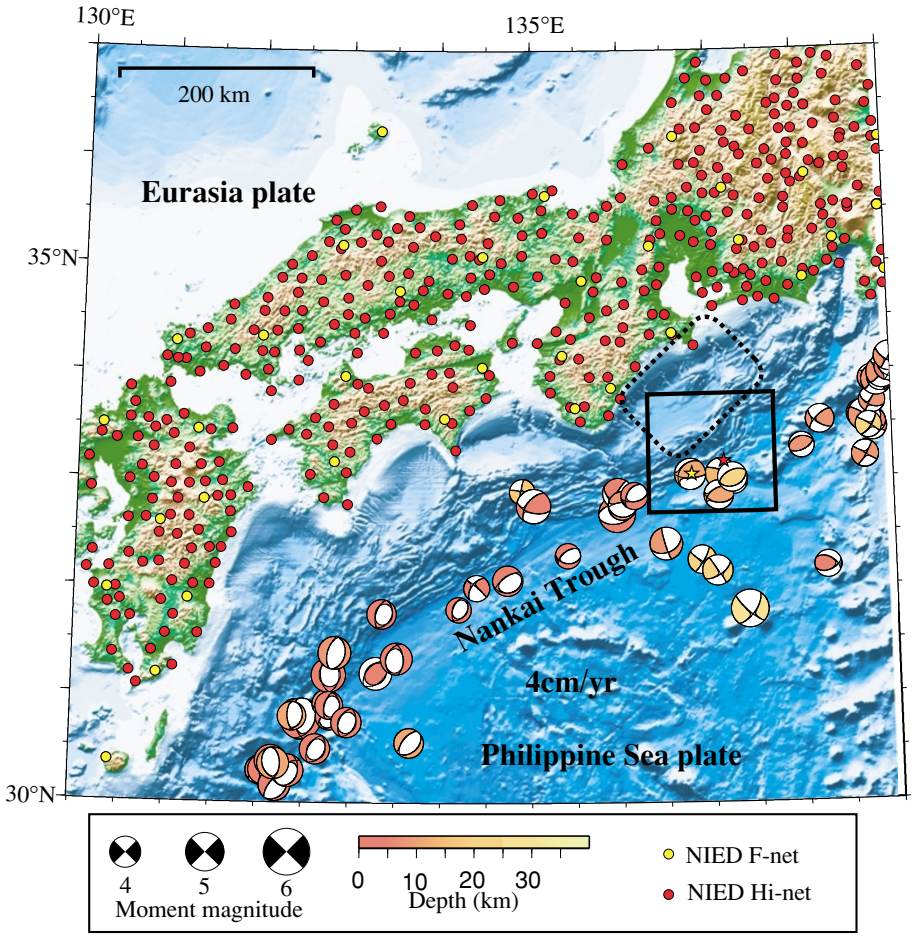

Fig. 1. Tectonic setting, station distribution in western Japan, and seismicity around the Nankai trough. Relative motion of the Philippine Sea plate to the Eurasia plate (Seno *et al*., 1993) is shown by the solid arrow. Focal mechanisms are only shown around the Nankai trough for earthquakes occurred from June 1997 to September 4, 2004. Yellow and red stars indicate epicenters of two main shocks with the moment magnitudes greater than 7 occurred on September 5, 2004 (JMA, 2004). Yellow and red circles show the NIED F-net and Hi-net stations. The rectangle is the focal area shown in the following figures. The broken line indicates the fault model of the 1944 Tonankai earthquake estimated by Kikuchi *et al*. (2003).

Table 1. Velocity and attenuation models.

Depth (km)	Thickness (km)	P velocity (km/s)	S velocity (km/s)	Density (kg/m^3)	Q_p	Q_s
0	3	5.50	3.14	2300	600	300
3	15	6.00	3.55	2400	600	300
18	15	6.70	3.83	2800	600	300
33	67	7.80	4.46	3200	600	300
100	125	8.00	4.57	3300	600	300
225	100	8.40	4.80	3400	600	300
325	100	8.60	4.91	3500	600	300
425	-	9.30	5.31	3700	600	300

and origin times in the JMA Catalog were used. VR was defined by

$$VR[\%] = 100 \times \sum_i w_i \left(1 - \frac{\int ((s_i(t) - o_i(t))^2 dt}{\int ((o_i(t))^2 dt}\right),$$

where $s_i(t)$ and $o_i(t)$ are the synthetic and observed waveforms, respectively. w_i is a constant weight that is proportional to the epicentral distance of station i. N is the number of stations.

3. Results

Between September 5 and October 31, 201 events with magnitudes exceeding 3.5 were listed in the JMA Catalog. We selected events if variance reduction exceeded 50 percent, more than 10 stations were used, and the centroid moment tensors of 94 events were determined. The moment magnitudes of these events ranged from 3.3 to 7.3. Source parameters for the main shocks exceeding M_W 7.0 are shown in Table 2 and are similar to those listed in the

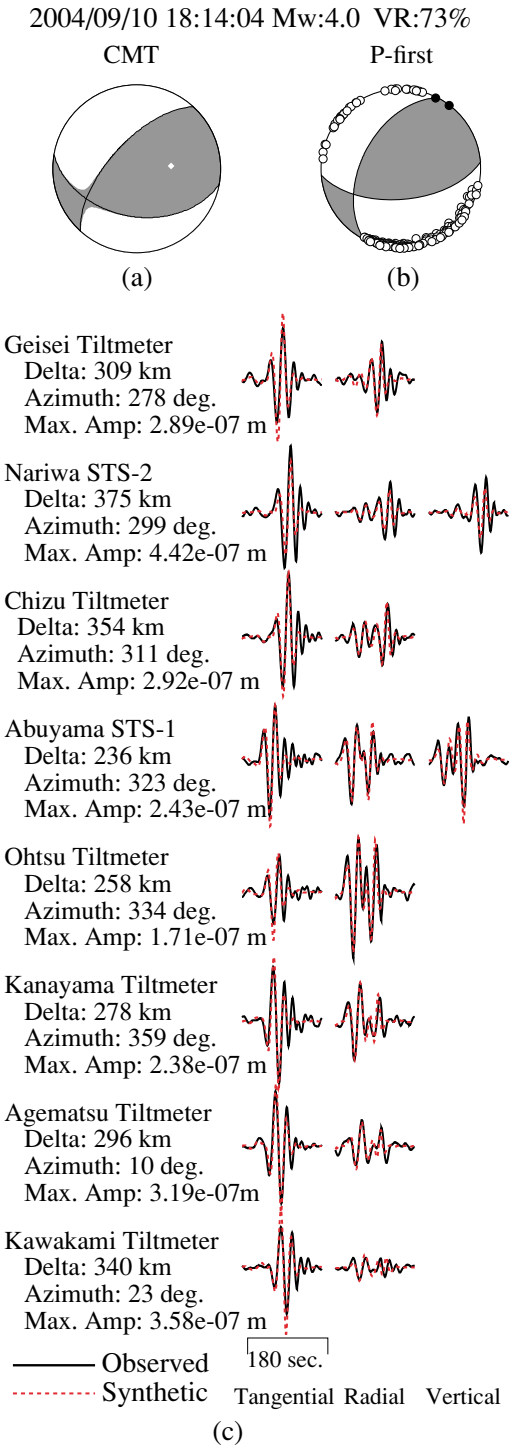

Fig. 2. Centroid moment tensor inversion. (a) The focal mechanism calculated by this approach. (b) The focal mechanism obtained from P-wave polarity analysis. Open and solid circles indicate the dilatational and compressional first motions for the P wave at Hi-net stations. (c) Observed and synthetic waveforms. The broken black and red line shows the observed and synthetic waveforms.

Harvard CMT Catalog.

Figure 2 shows an example of a centroid moment tensor inversion for a small earthquake with a magnitude of 4.0. The focal mechanism calculated by centroid moment tensor inversion was compared with that derived by P-wave polarity analysis using high-sensitivity seismometers at Hi-net stations (Figs. 2(a) and (b)). Full waveforms from P arrival to surface wave arrival were used in this study, with most of the waveforms observed being consistent with synthetic waveforms overall (Fig. 2(c)).

Figure 3 shows the distribution of centroid moment tensors and at least two types of earthquakes: the reverse-fault type (type-R) with a dip angle of 30–50 degrees that was similar to the main shocks, and another type (type-O) with a near-vertical nodal plane. We used Kagan's angle (Kagan, 1991) to show the similarity between the two different focal mechanisms. In order to classify the events into discrete categories based on the similarity of the mechanism characteristics of the larger main shocks and the aftershocks, we treated type-R events, which are similar to the main shock with a Kagan's angle of less than 30 degrees, and type-O events with a Kagan's angle exceeding 40 degrees separately. The type-R events include two main shocks that were distributed near the deformation front and ranged in depth between 5 km and 20 km. Conversely, many type-O events were scattered in the northern and western regions of the focal area at depths of less than 5 km.

Figure 4 shows examples of the centroid depths and moment tensor solutions as a function in VR. The results of type-R events show a clear peak in VR near the most optimal depths while the curve for type-O events is less pronounced. However, it is clear that type-O events occurred at depths shallower than 5 km in this example.

4. Discussion

Some reverse-fault events occurred in this region before the activity in 2004, with normal-fault events occurring near the deformation front in other regions along the Nankai trough (Fig. 1). Lay *et al.* (1989) demonstrated that the reverse-fault events occurred in the outer rise prior to the largest interplate thrust events, while tensional events generally followed interplate rupture. They also suggested that stresses in the outer rise might become compressional due to bending and slab-pull may be reduced when interplate thrusting was locked. The focal area and occurrence of type-R events was in the vicinity of, and due to, the asperity of the 1944 Tonankai earthquake.

In a cross section of the hypocentral distribution projected on a vertical plane using seismic survey data by Nakanishi *et al.* (2002), it is clear that the type-R events occur around the deformation front within the subducting Philippine Sea plate (Fig. 5). Type-R aftershocks, which have focal mechanisms and occur at depths that are similar to the main shocks, are only distributed beneath the deformation front. They were observed to extend east and west, which is consistent with the strike of the nodal planes of the main shocks. Type-O aftershocks, which have different nodal planes to those of the main shocks, are scattered throughout the entire area and occur at depths shallower than 5 km. These results suggest that the type-R aftershocks occurred on the same planes as the main shocks but that type-O aftershocks occurred on other planes. Interestingly, the distribution of type-R aftershocks may indicate expansion of the main shock faults.

Two clusters of type-O events can be seen in the northern and western parts of the focal area. Their focal depths

Table 2. Source parameters obtained for two main shocks.

Origin time (UT)	2004/09/05,10:07:07.50	2004/09/05,14:57:16.93
Fault mechanisms		
(Strike, Dip, Rake)[deg.]	(77.2, 43.8, 70.7)	(83.6, 37.4, 71.6)
Seismic moment [Nm]	4.3×10^{19}	9.9×10^{19}
Moment magnitude	7.0	7.3
Centroid latitude [degree]	33.00	33.08
Centroid longitude [degree]	136.79	137.00
Centroid depth [km]	9	8
Centroid time (UT)	2004/09/05, 10:07:17	2004/09/05, 23:57:44

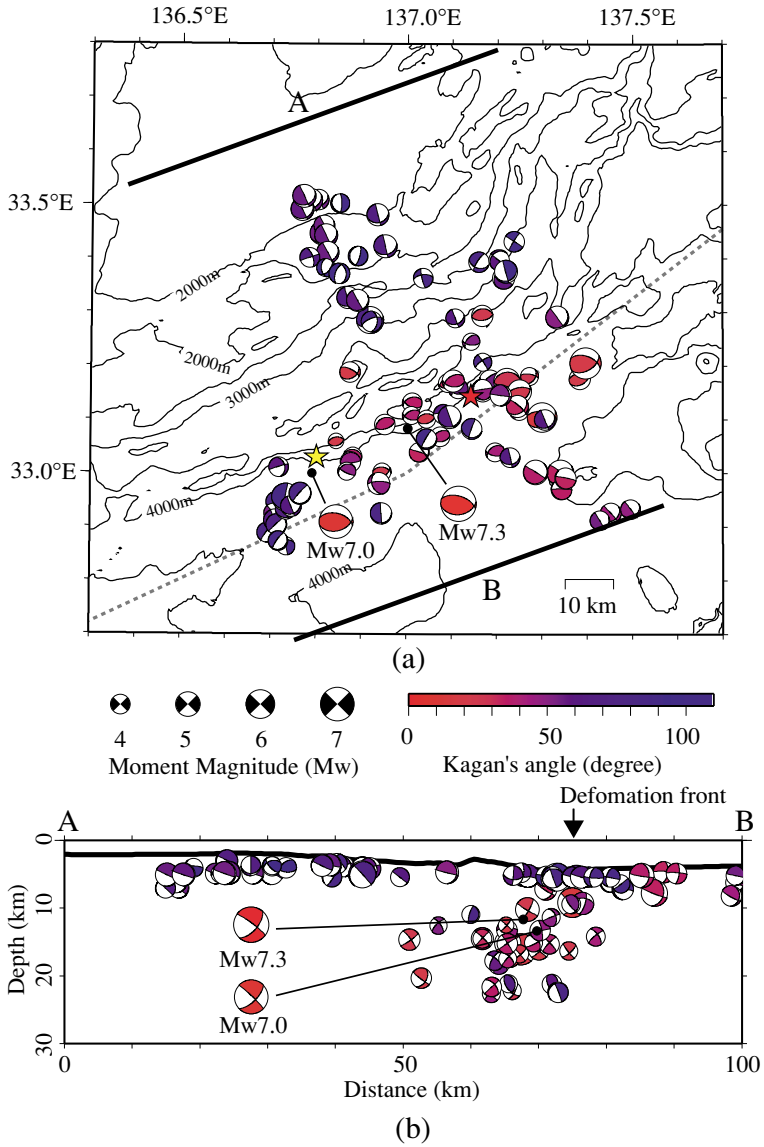

Fig. 3. Focal mechanism distribution. Color of moment tensors indicates the Kagan's angle. (a) Map-view. Yellow and red stars indicate epicenters of two main shocks of M_W 7.0 and 7.3, respectively. Bathymetric contour intervals are 500 m apart. The broken line represents the deformation front. (b) The cross section along A-B in (a). The bold line indicates the sea floor.

are markedly shallower than those of type-R events. Obara and Ito (2005) reported that the *S* coda parts of their events were relatively rich in low frequency components, that were manifested as surface waves. The distribution of type-O events in the northern and western parts of the focal area show clear lineaments with strikes of NNW-SSE and NE-SW, respectively (Fig. 5). These strikes are consistent with the strikes of nodal planes with the near-vertical dip angles

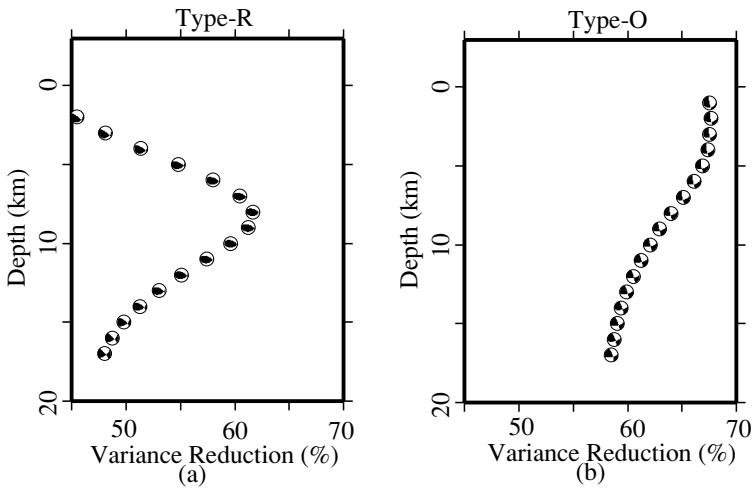

Fig. 4. Examples of variance reduction and moment tensor solutions plotted against centroid depth. (a) An example of a type-R event. (b) An example of a type-O event.

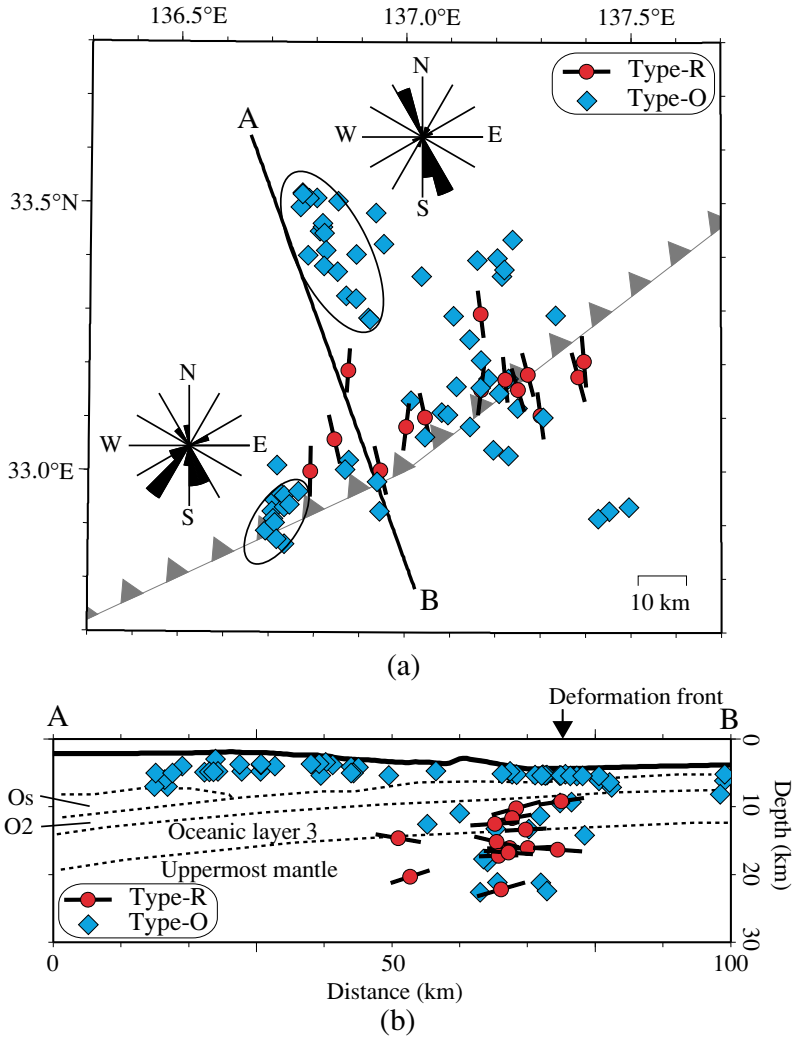

Fig. 5. Distributions of type-R and type-O events. Red circles and blue diamonds represent type-R and type-O events, respectively. Bold lines with red circles indicate the direction of *P* axes. (a) Map-view. The thin line with triangles shows the deformation front of the Nankai trough. Ellipses show typical clusters of type-O events. Two Rose diagrams show the percent frequency of strikes with near-vertical nodal planes, such as those of type-O events, within adjacent ellipses. (b) The cross-section along A-B. Broken lines show the boundary of geological interpretation by Nakanishi *et al.* (2002). Sw, Os, and O2 indicate the sedimentary wedge, the old accreted sediment, and oceanic layer 2, respectively.

of type-O events. Weak faults may exist in northern and western parts of the focal area and these might be triggered by large reverse-fault events that occurred beneath the deformation front.

5. Conclusion

We determined centroid moment tensors of two main shocks with moment magnitudes greater than 7 and intermediate size aftershocks by the centroid moment tensor inversion approach using the high-dense broadband seismic network. The results show that events, including the two main shocks, having characteristics of a reverse-fault with dip angle of 30 to 50 degrees are distributed around the deformation front of the Nankai trough at depths that range from approximately 5 to 20 km. On the other hand, strike-slip events or reverse-fault events with a near-vertical nodal planes are scattered at depths shallower than 5 km. Interestingly, the distribution of events the in northern and western parts of the focal area show clear lineaments with strikes of NNW-SSE and NE-SW, which agree with the strikes of nodal planes for those events.

Acknowledgments. We thank Dr. A. Velasco and an anonymous reviewer for comments on the manuscript. We would like to thank the Japan Meteorological Agency for providing us with the unified hypocenter catalog. We are grateful to Dr. M. Ishida, Dr. K. Kasahara, Dr. S. Hori, and Dr. H. Kumagai in NIED for valuable discussions. We thank Dr. A. Jin for polishing the language of this manuscript and for fruitful discussions. GMT (Wessel and Smith, 1995) was used to make the figures. Bathymetrical data provided by the Japan Oceanographic Data Center was used to draw the sea floor. This work was conducted as part of a project titled, "Operation of Seismic Observation Network" at the National Research Institute for Earth Science and Disaster Prevention.

References

Fukuyama, E., M. Ishida, D. S. Dreger, and H. Kawai, Automated seismic moment tensor determination by using on-line broadband seismic waveforms, *J. Seismol. Soc. Japan (Zisin)*, **51**, 149–156, 1998 (in Japanese with English abstract).

Hara, T., Change of the source mechanism of the main shock of the 2004 off the Kii peninsula earthquakes inferred from long period body wave data, *Earth Planets Space*, **57**, 179–183, 2005.

Hashimoto, M., K. Onoue, F. Ohya, Y. Hoso, K. Segawa, K. Sato, and Y. Fujita, Crustal deformations in Kii peninsula associated with the SE off the Kii peninsula earthquake sequence of September 5, 2004 derived from dense GPS observations, *Earth Planets Space*, **57**, 185–190, 2005.

Japan Meteorological Agency, *The Seismological and Volcanological Bulletin of Japan*, Japan Meteorological Agency, Tokyo, 2004.

Kagan, Y. Y., 3-D rotation of double-couple earthquake sources, *Geophys. J. Int.*, **106**, 709–716, 1991.

Kikuchi, M., M. Nakamura, and K. Yoshikawa, Source rupture processes of the 1944 Tonankai earthquake and the 1945 Mikawa earthquake derived from low-gain seismograms, *Earth Planets Space*, **55**, 159–172, 2003.

Lay, T., L. Astiz, H. Kanamori, and D. H. Christensen, Temporal variation of large intraplate earthquakes in coupled subduction zones, *Phys. Earth Planet. Inter.*, **54**, 258–312, 1989.

Nakanishi, A., H. Shiobara, R. Hino, J. Kasahara, K. Suyehiro, and H. Shinohara, Crustal structure around the eastern end of coseismic rupture zone of the 1944 Tonankai earthquake, *Tectonophysics*, **354**, 257–275, 2002.

Obara, K. and Y. Ito, Very low frequency earthquakes excited by the 2004 off the Kii peninsula earthquakes: A dynamic deformation process in the large accretionary prism, *Earth Planets Space*, this issue, **57**, 321–326, 2005.

Okada, Y., K. Kasahara, S. Hori, K. Obara, S. Sekiguchi, H. Fujiwara, and A. Yamamoto, Recent progress of seismic observation networks in Japan—Hi-net, F-net, K-NET, and KiK-net, *Earth Planets Space*, **56**, xv–xxviii, 2004.

Satake, K., T. Baba, K. Hirata, S. Iwasaki, T. Kato, S. Koshimura, J. Takenaka, and Y. Terada, Tsunami source of the 2004 off the Kii Peninsula earthquakes inferred from offshore tsunami and coastal tide gauges, *Earth Planets Space*, **57**, 173–178, 2005.

Seno, T., S. Stein, and A. E. Grippe, A model for the motion of the Philippine Sea plate consistent with NYVEL-1 and geological data, *J. Geophys. Res.*, **98**, 17941–17948, 1993.

Shiomi, K., K. Obara, S. Aoi, and K. Kasahara, Estimation on the azimuth of the Hi-net and KiK-net borehole seismometers, *J. Seismol. Soc. Jpn. (Zisin)*, **56**, 99–110, 2003 (in Japanese).

Utsu, T., *Seismology, second edition*, 310 pp., Kyoritsu Syuppan, Tokyo, 1984 (in Japanese).

Wessel, P. and W. H. F. Smith, New version of the generic mapping tools released, *EOS Trans. AGU*, **76**, 329, 1995.

Y. Ito (e-mail: yito@bosai.go.jp), T. Matsumoto, H. Kimura, H. Matsubayashi, K. Obara, and S. Sekiguchi